POAC'15
Trondheim, Norway

Proceedings of the 23rd International Conference on
Port and Ocean Engineering under Arctic Conditions
June 14-18, 2015
Trondheim, Norway

AN EFFICIENT NUMERICAL MODEL FOR MARINE ICING

E. S. Hansen [1] and S. H. Teigen [1]
[1]Statoil ASA, Bergen, Norway

ABSTRACT

The implementation of a numerical model for predicting severity and frequency of marine icing, based on existing theory of sea spray generation and freezing, is described. The model is time-dependent and takes into account salt expulsion and run-off of the freezing sea water. Spray shielding by structural elements is also taken into account with a novel algorithm. The model is fully three-dimensional, and will calculate the spatial distribution of icing rate and accumulated ice thickness on a given vessel or offshore structure. The model is numerically efficient and well suited for deriving extreme values of marine icing for early assessment of icing severity in arctic offshore projects. The numerical model is applied in a case study with a semi-submersible structure in the Barents Sea. A sensitivity study is also presented, along with a comparison of icing estimates with actual icing observations from a drilling rig in Cook Inlet, Alaska.

INTRODUCTION

Icing can have adverse effects on vessels and platforms operating in cold climate regions, leading to reduced operability, blocking of mechanisms, slippery deck and ladders, inoperability of evacuation systems, and in the worst case compromise the structural integrity or stability, which could cause the loss of the vessel/platform and all lives aboard. The two categories of icing are

- Atmospheric icing, due to snow, freezing rain, frost or fog.
- Marine icing (or sea spray icing), due to ship/wave interaction (collision spray), or spume blown from wave crests (white cap spray)

Although atmospheric icing can be extremely dangerous for aviation, sea spray icing is usually the dominating source of ship icing (up to 90% of the mass in sub-arctic seas (Løset, 2006)). Within the ice edge, where surface waves are quickly attenuated, the relative contribution from atmospheric icing is more substantial. Early models of icing were based on statistical relations between icing events and environmental conditions (see e.g. Overland (1986)). Even today, the icing warnings issued by meteorological services are based on these models. After the advent of modern computer resources, attempts have been made to make more realistic physical models (Horjen (1990), Blackmore & Lozowski (1993)).The physical properties (density, salinity, porosity, etc.) of the accreted ice have been measured in various field studies (Ryerson (2000), Kulyakhtin (2013)).

Icing on drilling rigs and production units also poses a potential hazard for arctic oil and gas exploration and field developments, which has caused a renewed interest in the subject (Shipilova, et al. (2012), Kulyakhtin & Tsarau (2014)).

Based on the models described by Horjen (1990) and Lozowski, et al. (2000), Hansen (2012) implemented a computationally efficient three-dimensional, time dependent model of marine icing. The model is named NuMIS (Numerical Model for Icing and Snow). The present paper describes the theory behind the model, implementation, a case study and comparison with a real icing event.

THEORY

The theory behind the spray and freezing model is discussed at length by e.g. Horjen (1990) and Hansen (2012).

Collision spray

In 1983-84, a measurement campaign of sea spray was performed on the semi-submersible drilling rig "Treasure Scout", as described by Jørgensen (1984). The resulting data was used by Horjen & Vefsnmo (1985), together with physical considerations, to develop an equation for the time-averaged collision spray flux profile $\bar{R}_{wave}(z)$ given by

$$\bar{R}_{wave}(z)\left[\frac{\mathrm{kg}}{\mathrm{m^2 s}}\right] = M_0 U_{10}\left\{1-(1-10^{-2}U_{10})\exp\left[-\left(\frac{4z'+2}{9}\right)^2\right]\right\}\exp(-k_e z'^2) \qquad (1)$$

where

$$M_0 = 2\,\pi\cdot 10^{-4}\quad \frac{\mathrm{kg}}{\mathrm{m^3}}$$

$$k_e = 5.88\cdot 10^{-2}\ U_{10}^{\frac{2}{3}}$$

$$z' = \frac{2z}{H_s} - 1.$$

Here, U_{10} is the wind speed at 10 m above mean sea level, z is the height above mean sea level, and H_s is the significant wave height.

Equation (2) is the time-averaged spray flux based on measurements performed at the windward side of a platform leg. "Time-averaged" here refers to the fact that measurements were taken over many spray periods, whereas the spray flux in the time-dependent model should be altered to come in short bursts with no spray in between. It was observed by Jørgensen (1985) that the sea spray flux on the leeward side was approximately 10% of the flux on the windward side. For the purpose of the present model, it will be assumed that equation (2) is the average flux over the windward side. It will also be assumed that the spray flux has a maximum where the leg is normal to the wind direction, that the spray flux varies continuously, and that it is equal to 10% of the windward average on the entire leeward side. This gives the following modified form for the time-dependent spray flux $R_{wave}(z, t)$ during one spray period:

$$R_{wave}(z,t) = \begin{cases} \frac{\tau_p}{\tau_s}\bar{R}_{wave}(z)\left(0.1+0.9\frac{\pi}{2}\max\left[\cos\left(-\frac{\boldsymbol{U}}{|\boldsymbol{U}|}\cdot\boldsymbol{n}\right),0\right]\right), & t\le\tau_s \\ 0, & \tau_s < t \le \tau_p \end{cases} \qquad (2)$$

where τ_p is the spray period, τ_s is the duration of a single spray, $\boldsymbol{U}$ is the wind speed vector, and $\boldsymbol{n}$ is the normal vector of the local surface.

White cap spray

The white cap spray flux $R_{wind}(z)$ is given by Jones & Andreas (2012) as

$$R_{wind}(z) = \frac{4}{3}\pi\rho_w U(z) \begin{cases} 7 \cdot 10^4 U_{10}^2 \int_{5\mu\mathrm{m}}^{100\mu\mathrm{m}} F(r,z)E(r)\ \mathrm{d}r, & U_{10} < 19\ \mathrm{m/s} \\ 30 U_{10}^4 \int_{5\mu\mathrm{m}}^{200\mu\mathrm{m}} F(r,z)E(r)\ \mathrm{d}r, & U_{10} \geq 19\ \mathrm{m/s} \end{cases} \quad (3)$$

where ρ_w is the sea water density, $U(z)$ is the wind speed at height z, $E(r)$ is the collision efficiency between droplets of radius r and the local surface. For the purpose of this model, the droplets are assumed to have a high inertia, and the collision efficiency is simulated by simply adjusting for the orientation of the surface as such:

$$R_{wind}(z) = \frac{4}{3}\pi\rho_w U(z) \max\left[\cos\left|-\frac{\boldsymbol{U}}{|\boldsymbol{U}|}\cdot\boldsymbol{n}\right|, 0.1\right] \begin{cases} 7 \cdot 10^4 U_{10}^2 \int_{5\mu\mathrm{m}}^{100\mu\mathrm{m}} F(r,z)\ \mathrm{d}r, & U_{10} < 19\ \mathrm{m/s} \\ 30 U_{10}^4 \int_{5\mu\mathrm{m}}^{200\mu\mathrm{m}} F(r,z)\ \mathrm{d}r, & U_{10} \geq 19\ \mathrm{m/s} \end{cases} \quad (4)$$

The minimum directional factor of 0.1 is enforced to avoid the unphysical result of a surface being completely unexposed to white cap spray.

The function $F(r,z)$ is given by

$$F(r,z) = \begin{cases} r^2 \left(\frac{z}{1\mathrm{m}}\right)^{-\frac{v_g(r)}{0.4u_f}} \exp\left\{-\frac{1}{2}\left[\ln\left(\frac{r}{0.3\mu\mathrm{m}} - 2.8\right)\right]^2\right\}, & U_{10} < 19\ \mathrm{m/s} \\ r^2 \left(\frac{z}{0.5H_s}\right)^{-\frac{v_g(r)}{0.4u_f}} \exp\left\{-\frac{1}{2}\left[\ln\left(\frac{r}{0.3\mu\mathrm{m}} - 4\right)\right]^2\right\}, & U_{10} \geq 19\ \mathrm{m/s} \end{cases} \quad (5)$$

where v_g is the is the terminal velocity of a droplet with radius r and u_f is the friction velocity.

Icing rate

The time-dependent spray flux for each spray period is calculated by:

$$\begin{aligned} R(0 < t \leq \tau_s) &= R_{wave}S_{wave} + R_{wind}S_{wind}, \\ R(\tau_s < t < \tau_p) &= R_{wind}S_{wind}. \end{aligned} \quad (6)$$

In other words, a step function where the flux is initially spray and wind flux for the spray duration τ_s, and decreasing to just the wind spray for the remainder of the spray period.

The sea spray temperature T_{spray} is the flux-weighted average of the collision spray temperature (assumed equal to the sea surface temperature) and the wind spray temperature (assumed equal to the air temperature). Thus,

$$T_{spray}(0 < t < \tau_s) = \frac{R_{wave}T_s + R_{wind}T_a}{R_{wave} + R_{wind}},$$
$$T_{spray}(\tau_s < t < \tau_p) = T_a. \quad (7)$$

where T_s is the sea surface temperature and T_a is the air temperature. This implies that the cooling of collision spray droplets after being generated and before impinging on the structure is neglected, while the much smaller droplets of the wind spray are assumed to already be cooled down to the air temperature. The air temperature available in the hindcast data is the temperature 2 meters above the sea surface. The air temperature can be somewhat cooler further up, but a vertical temperature profile is not implemented in the model.

For each panel, the time series of spray flux and temperature are used to calculate the icing rate. The exact details of these calculations were explained by Hansen (2012), but it is based on the method used by Horjen (1990). In short, the model assumes a layer of brine present on the surface, and solves the differential equations for mass, salt and heat content of the brine layer:

$$\frac{\partial X}{\partial t} + \nabla_t \cdot (\boldsymbol{v}_b X) = R - I, \quad (8)$$
$$c_b X \left(\frac{\partial}{\partial t} + \boldsymbol{v}_b \cdot \nabla_t\right) T_b = Q + (1-\sigma) l_f I, \quad (9)$$
$$\frac{X}{S_b}\left(\frac{\partial}{\partial t} + \boldsymbol{v}_b \cdot \nabla_t\right) S_b = I(1-\sigma) - R\left(1 - \frac{S_w}{S_b}\right). \quad (10)$$

Here, X is the local mass of brine per unit area [kg/m^2], T_b is the brine temperature and S_b is the brine salinity (in parts per thousand). The parameter $\boldsymbol{v}_b$ is the velocity of the brine film, and ∇_t is the differential operator in the tangential direction (i.e. along the direction that the brine will move in). The spray flux R is given by equation (8). The parameter I is the rate of accretion formation [kg/m^{2}s], which includes both ice and entrapped brine. Also, c_b is the specific heat capacity of the brine, σ is the fraction of entrapped brine in the accretion (assumed to be constant equal to 0.34 by Horjen (1990)), l_f is the latent heat of freezing and S_w is the salinity of sea water. Note that mass flux due to evaporation is neglected.

The heat flux from the brine layer at the surface is given by

$$Q = Q_c + Q_e + Q_r + Q_s \quad (11)$$

where the heat fluxes are conductive (Q_c), evaporative (Q_e), radiative (Q_r) and sensible heat (Q_s) fluxes. The heat fluxes are defined as positive when the heat goes from the brine layer to the air, i.e. when the brine layer loses heat. The different heat flux terms are calculated from the parameterizations from Lozowski, et al. (2000). However, the model uses a different convective heat transfer coefficient, in order to be relevant for larger surfaces. For cylinders, the model uses the following equation from Churchill & Bernstein (1977) :

$$h = \frac{k_a}{D}\left(0.3 + \frac{0.62 Re_D{}^{\frac{1}{2}} Pr^{\frac{1}{3}}}{\left(1+\left(\frac{0.4}{Pr}\right)^{\frac{2}{3}}\right)^{\frac{1}{4}}}\left(1+\left(\frac{Re_D}{282000}\right)^{\frac{5}{8}}\right)^{\frac{4}{5}}\right) \quad (12)$$

Here, k_a is the thermal conductivity of air, D is the diameter of the cylinder, Pr is the Prandtl number of air, Re_D is the Reynolds number of the cylinder given by

$$Re_D = U_{10} D / \nu_a$$

and ν_a is the kinematic viscosity of air. For planar components, the heat transfer coefficient is given by

$$h = \frac{U_{10}^{0.8}}{L^{0.2}}\left(8 - 4.4 \max\left(\frac{\boldsymbol{U}}{|\boldsymbol{U}|}\cdot \boldsymbol{n}, 0\right)\right) \quad (13)$$

where $\boldsymbol{n}$ is the normal vector of the surface. Here, L is the horizontal length of the surface. These equations are based on the average heat transfer coefficient from CFD modelling of a 10x10x10 m cube (Defraeye, et al., 2010), adjusted to fit an $L^{-0.2}$ relation, which is the expected size dependency of structures of this size. It has also been adjusted to be continuous as a function of the surface orientation $\boldsymbol{n}$, with the largest heat transfer at the front and at the sides.

IMPLEMENTATION

Shielding

The model uses a simplified model for estimating structural shielding. For practical purposes, it will be assumed that the spray droplets have a high inertia – i.e. the droplet trajectory is calculated as if there is no structure present, and it is assumed the droplet hits the first panel that intersects the droplet trajectory. Panels may therefore be shielded from spray, completely or partially, by other panels. In the model, this effect is realized by the previously mentioned shielding factor S, which can be between 0 (completely exposed) and 1 (completely shielded).

In order to calculate S, the trajectory for droplets generated by collision spray is first calculated from Lozowski, et al. (2000), which gives the droplet equation of motion as

$$\frac{\mathrm{d}\boldsymbol{v}_d}{\mathrm{d}t} = -\frac{3}{4}\frac{C_d}{D}\frac{\rho_a}{\rho_w}\,|\boldsymbol{v}_d - \boldsymbol{U}_{10}|\,(\boldsymbol{v}_d - \boldsymbol{U}_{10}) - \boldsymbol{g}\left(\frac{\rho_a}{\rho_w} - 1\right). \quad (14)$$

Here, $\boldsymbol{v}_d$ is the droplet velocity, C_d is the drag coefficient, D is the droplet diameter, ρ_a and ρ_w are the air and water density respectively, and $\boldsymbol{g}$ is the gravitational acceleration. Droplets generated by collision spray are assumed to have a constant diameter of D = 1.75mm,

Droplets generated by white cap spray are assumed to be small and travel horizontally (i.e. $\boldsymbol{v}_d = \boldsymbol{U}$). Keep in mind that the simplified shielding model for white cap spray replaces the collision efficiency described by Jones & Andreas (2012), i.e. the collision efficiency for cylinders from this article is not used.

The shielding factor for collision spray is calculated from the following algorithm:

1. It is assumed the spray will originate at an imaginary vertical surface that follows the outer perimeter of the vessel as seen from above.
2. The droplet trajectory from this surface to all panels in the geometrical model is calculated from equation (14).
3. The panels are sorted by their distance (along the droplet trajectory) to the vertical surface that follows the perimeter of the vessel.
4. One by one, the panels are projected along the droplet trajectory onto this surface, and compared with the union of all previously projected panels.
5. The shielding factor is given by the area of the intersection between the projected panel and the union of all previously projected panels, divided by the area of the projected panel.

The shielding factor for wind cap spray is calculated by a similar algorithm, except the droplet trajectory is assumed to be a horizontal line following the wind direction.

This is described in more detail by Hansen (2012). The exact method for finding which panels/polygons of the geometrical model are closest to the spray (step 3) is as such:

- If *all* corners of polygon A are closer to the spray than *all* corners of polygon B, then polygon A is closer to the spray than polygon B and vice versa.
- If only *some* corners of polygon A are closer to the spray than the corners of polygon B, an additional check must be made.
- This is done by finding the intersection between the projection of polygon A and polygon B, and then projecting the corners of the intersection polygon back along the droplet trajectory onto polygon A and polygon B respectively. A check is then made on each projected corner. If *any* corner of the intersection polygon projected onto A is closer than the same corner projected onto B, then polygon A is closer to the spray than polygon B, and vice versa.

Any panel that is positioned on the vessel hull (or vessel legs, in the case of a semi-submersible) are considered unshielded by definition.

Runoff

The model includes the ability for panels to give or receive brine film runoff from neighbouring panels. For practical purposes, it will be assumed that runoff is driven solely by gravity rather than wind shear. This means runoff will always travel downwards, and that horizontal panels will not give runoff. Also, runoff will not generally travel between different surface components in the geometrical model (i.e. from a vertical wall to a horizontal surface), because the grid points on the two surfaces will generally not be aligned.

As part of the pre-processing of a new geometrical model, each panel/polygon will be assigned runoff as follows:

- Assume a quadrilateral polygon A consisting of nodes N_1, N_2, N_3 and N_4. The polygon consists of edges $\boldsymbol{E_{1\text{-}2}}$, $\boldsymbol{E_{2\text{-}3}}$, $\boldsymbol{E_{3\text{-}4}}$ and $\boldsymbol{E_{4\text{-}1}}$.

- The edges are checked if they bound the polygon along the bottom (i.e. along the lower vertical direction). A simple check consists of taking the cross product of the polygon normal $\boldsymbol{N}$ and the edge. For example, if the cross product ($\boldsymbol{N}$ x $\boldsymbol{E_{1\text{-}2}}$) has a **positive** *z* value, it means the edge bounds the polygon along the bottom.
- For each such edge, it is checked if any other polygon in the geometry shares the edge – i.e. if any other polygon has an edge consisting of the same nodes. If such polygons are found, these polygons will receive runoff from polygon A. If polygon A gives runoff over several edges, the runoff will be distributed proportional to the horizontal length of each edge.

Icing rate

The icing rate is calculated for three subsequent spray periods – the two first periods are calculated merely to initialize the system (by providing initial values for water content and salt content, which otherwise are not well defined), and the results are discarded. The icing rate resulting from the third period is averaged over the period, and this average icing rate is assumed to be constant throughout each time step in the time series of metocean variables, e.g. 3 hour intervals for the NORA10 hindcast archive.

A flow chart of the calculation process used in NuMIS is presented in Figure 1.

Wave washing

"Wave washing" refers to the physical removal of accumulated ice due to wave actions on the structure. For the purpose of this model, it will be assumed that all ice on panels below 90% of the height above mean surface level of the highest expected wave in a given 3-hour period will be removed. Specifically, this height is given by

$$z_{wash} = 0.9\frac{H_s}{2}\sqrt{\frac{\ln\left({}^{10800}/_{T_m}\right)}{2}} \qquad (15)$$

where T_m is the mean wave period. For instance, for a significant wave height of 2 meters and an average wave period of 6 seconds, the wave washing height is 1.74 m above the mean water level.

CASE STUDY

For the case study, a simplified semi-submersible drilling rig has been used. The geometrical model consists of 16560 panels, and is manually divided into sections that are chosen as being either planar or cylindrical, and each section has a (manually chosen) characteristic length associated with it. For cylindrical components, this is the diameter; for planar components, this is the longest of the horizontal side lengths of the object. The geometry is illustrated in Figure 2. For all constants, or variables that are assumed constant (e.g. seawater salinity, latent heat of freezing, etc.) the values are the same as those used by Hansen (2012).

The shielding calculations described in the preceding section are performed as part of the pre-processing. The shielding is calculated for a given set of wind speeds and wind directions. When running the model itself, the model will use the wind speed and wind direction from the hindcast data and find the shielding factors by interpolating the shielding factors for the closest wind speeds and wind directions in the data from the pre-processing. The case study uses a resolution of 2 m/s for wind speed and 30° for wind direction. The shielding pre-

processing for this model can be performed on a single laptop computer in less than one hour, assuming the calculations are parallelized efficiently between the different processors. An example of the results of the shielding calculations is shown in Figure 3. Notice that the platform legs, as mentioned in the previous section, are unshielded by definition.

The model has been run using meteorological and oceanographic data from the Nora10 hindcast model (Reistad, et al., 2010) for the location 73.25°N and 25.10°E in the Barents Sea, for the period 1957-2014. The location is shown in Figure 4. It is assumed that the platform is stationary throughout the whole time period, i.e. it does not rotate, and the *x* axis as indicated in Figure 2 is directed towards north. The time series of total accumulated ice mass on the structure is shown in Figure 5, along with the maximum value for each icing season.

For this particular case, the computation time would be around 10-15 hours for the whole period (1957-2014) when run on a single computer. However, the model is easily parallelized on several processsors, since the icing estimates each winter are independent from all other winters. Thus, the run time will be approximately inversely proportional with the number of processors available. The computation time obviously increases with higher panel resolution and higher resolution in the metocean data.

In Figure 6, the distribution of ice thickness on the structure during the event with the highest total mass of ice in the time series (11th of March 1998) is shown, using both a linear and logarithmic colour scale. Note that zero ice thickness is coloured in grey.

COMPARISON WITH OBSERVATIONS

Although the number of well-documented observations of icing is limited, particularly on drilling rigs and large vessels, there are some data available. This article will compare the results from the numerical icing model with icing observations done on the semi-submersible drilling rig *Ocean Bounty*, operating in Cook Inlet in Alaska during the 1979-1980 winter season. The icing observations are described by Nauman (1984), and the meteorological and wave data along with approximate icing rates are reported by Jones & Andreas (2009).

The *Ocean Bounty* platform, according to Nauman (1984), has a leg diameter of 7.47 m and a leg height of 15.24 m (i.e. the bottom of the main deck is at this height) during drilling conditions. For the comparison, a cylinder with a diameter of 7.47 m and a total height of 30 m was modelled. The numerical model was used to calculate time series of icing rate (not accumulated ice thickness, since it was the approximate icing rate that was registered by the crew). Two heights were chosen, 5 m and 15 m above sea level, and the *maximum* icing rate registered on the panels placed at the two respective heights were examined. The results are shown in Figure 9, where the time series of maximum estimated icing rate at 5 m and 15 m above surface level are plotted alongside the approximate icing rates registered on the vessel. Since the observations were likely done on the main deck, the rates at 15 m as are most relevant for the comparison.

SENSITIVITY STUDY

In order to assess the sensitivity of the icing results from the model to the different weather and wave parameters, the model was run using the same semi-submersible geometry as shown in Figure 2, using the following parameters as a “base case”:

Table 1: Parameters used as a base case for the sensitivity study.

Parameter	U_{10}	H_s	T_a	T_s	RH	τ_p
Value	20 m/s	5 m	-10 °C	3 °C	0.8	10 s

where *RH* is the relative humidity. The total icing rate (i.e. for the entire structure) for this base case was calculated to be 6.56 tonnes/hour. Each of the parameters (wind speed, wave height, air temperature and sea surface temperature) is then allowed to vary while the other parameters are kept constant. The results are shown in Figure 7. Sensitivity to relative humidity and significant wave period was also checked, but found to be of minor importance.

DISCUSSION

Model limitations

In order to be numerically efficient, the model does not take into account:

- The changes in the distance to the free surface caused by the motion of the structure itself
- That ice can start to break off due to its own weight
- Turbulent transport of spray, which can deposit droplets on the lee-side of structural elements

These processes have a potential impact on the total icing on a structure, but are probably less influential than the uncertainty in the incoming spray flux. The spray flux will differ between different structure shapes in variable sea states and wind conditions and available data sets for different structures are very few. Modelling and data collection in relation to heat loss from large structures like an offshore platform is also a subject that has not received much attention, and still have a substantial impact on icing.

Comparison with observations

As is shown in the figure, the estimated icing rates are usually of the same order of magnitude as the approximate observed rates. However, there is one period in particular (approximately from 8th of December to 15th of December, 1979), where significant icing is predicted but where there are no observations. It is possible that there was icing on the rig during this period, but that the observations were not recorded for this period – one may even speculate if this icing event (if it did occur) may have triggered the registrations of icing afterwards.

Note that the available data on *Ocean Bounty* is for icing rate, whereas the main application of the numerical model for engineering purposes is the accumulated ice load. It would be useful to additionally compare the output from the model with a well-documented time series of ice thickness.

Sensitivity study

The sensitivity study indicates that the icing increases slower than linearly with wind speed for wind speeds below 18-19 m/s, and then increases faster than linearly for higher wind speeds. Note that here, the wave height is held constant and is therefore independent from wind speed. For lower wind speeds, the wave collision spray is dominant and the icing is thermally limited – thus, the icing rate dependency on wind speed is approximately the same as the heat loss coefficient dependency on wind speed, and this dependency is less than linear. For higher wind speeds, the white cap spray dominates, and the total spray flux (and thus the

icing rate) increases faster than linearly with wind speed, as seen in equation (3). The apparent discontinuity at 19 m/s is due to the discontinuity in equation (5).

The study suggests that icing rate is approximately proportional to wave height. The reason for the apparent jagged form of the curve is due to limited vertical resolution in the modelled geometry. As for the air temperature dependency, the icing rate is strongly dependent on air temperature when air temperature is > -10°C, but the dependency decreases as air temperature becomes lower. This is to be expected, as more areas on the structure become mass-limited rather than thermally limited for lower air temperatures. The study suggests that the icing rate is not very sensitive to sea surface temperature – this is a major difference from e.g. the Overland algorithm for icing calculations (Overland, 1986), which predicts a strong sea surface temperature dependency.

The model is also expected to be sensitive to the brine fraction σ, in this model assumed to be constantly 0.34. An increasing brine fraction will increase the ice accretion mass, but also affect the water and salt transport used to solve for the icing rate. Sensitivity for brine fraction has not been checked.

SUMMARY

The development of the Numerical Model for Icing and Snow (NuMIS) is described. The underlying equations used in the model are presented, and the simplified implementation of a practical and numerically efficient model used that may be used on long time series for three-dimensional geometrical models is described. A case study of a simplified semi-submersible drilling rig in the Barents Sea is presented, with both time series of accumulated ice and the ice thickness distribution during the worst estimated icing event from the time series. The model is fast and able to calculate icing for time periods long enough to be useful in extreme value statistics. A comparison between the model estimates and a registered heavy icing event on the drilling rig Ocean Bounty in Cook Inlet during the winter of 1979-80 is also presented. The comparison indicates a reasonably good correspondence between estimated and observed values. Finally, a sensitivity study is presented, indicating that wind speed, wave height and air temperature are the main parameters affecting icing rate, with sea surface temperature being less important.

FIGURES

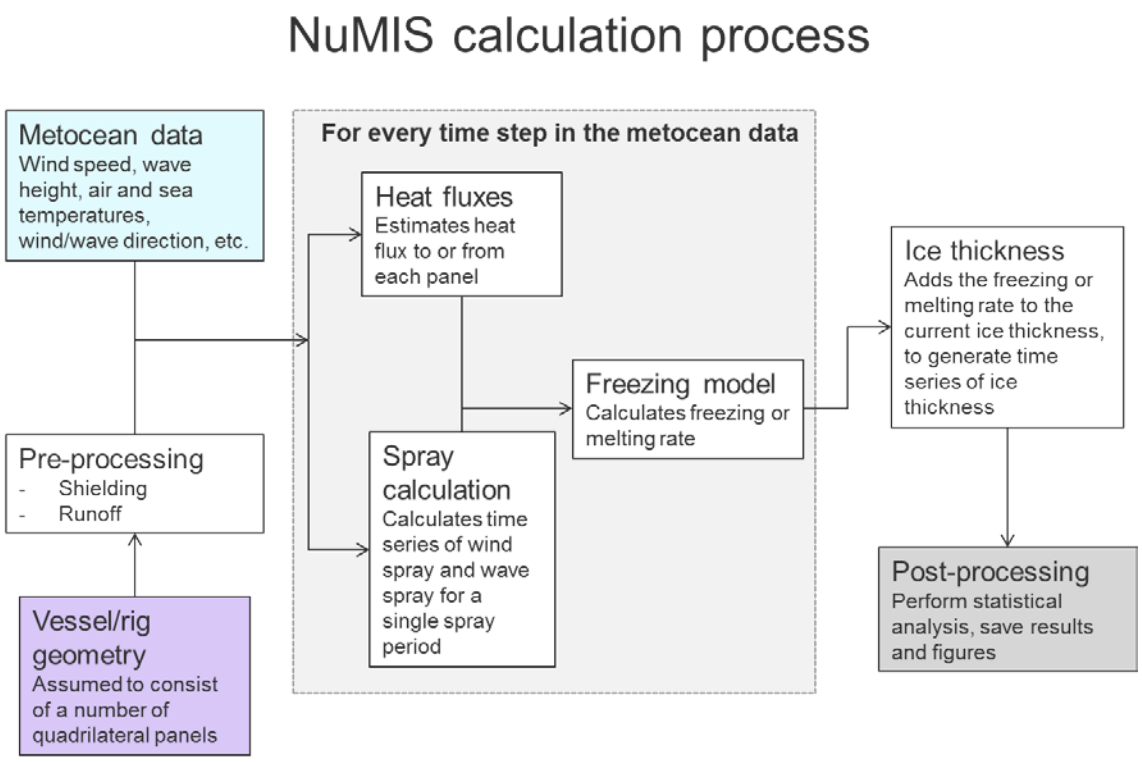

Figure 1. Flow chart of the calculation process used in the NuMIS model.

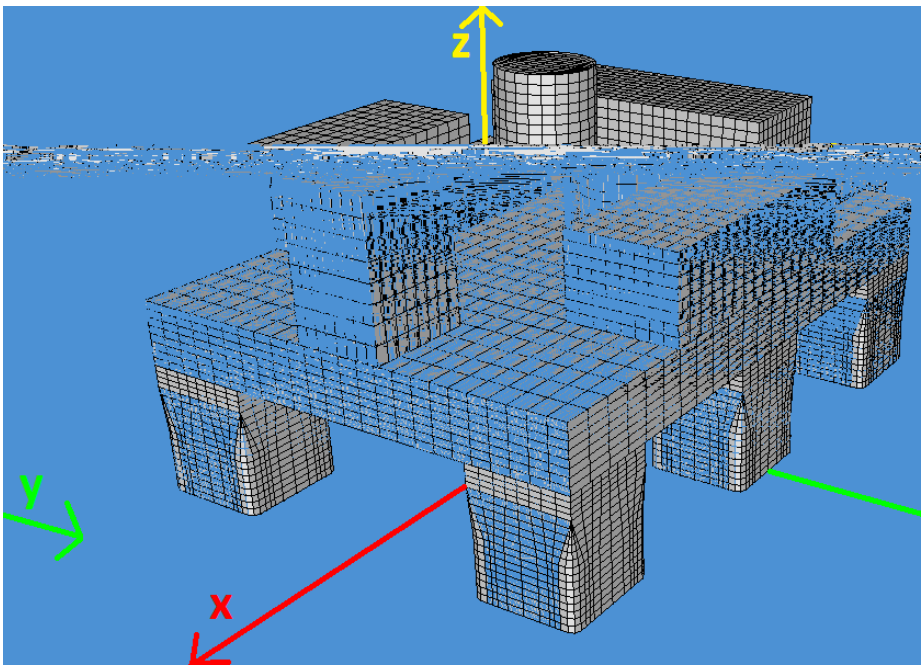

Figure 2. Illustration of the simplified semi-submersible used in the case study. The numerical panels shown in the illustration are as is used in the calculations and give an indication of the resolution of the model.

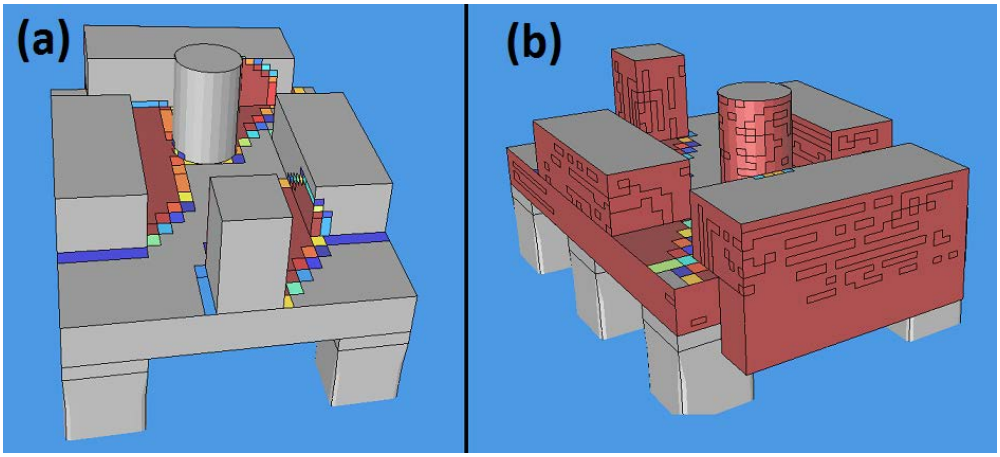

Figure 3. Illustration of the results from the shielding model for the geometry used in the case study, both seen from (a) along the incoming wind direction and (b) against the incoming wind direction . The wind direction is 30° from starboard (assuming fore is directed along the *x* axis in Figure 1), and the wind speed is 10 m/s. Grey indicates completely unshielded, whereas the colour scale goes from slightly shielded (blue) to completely shielded (red). Note that there are some artefacts along the component edges, due to the polygons from different components not being aligned.

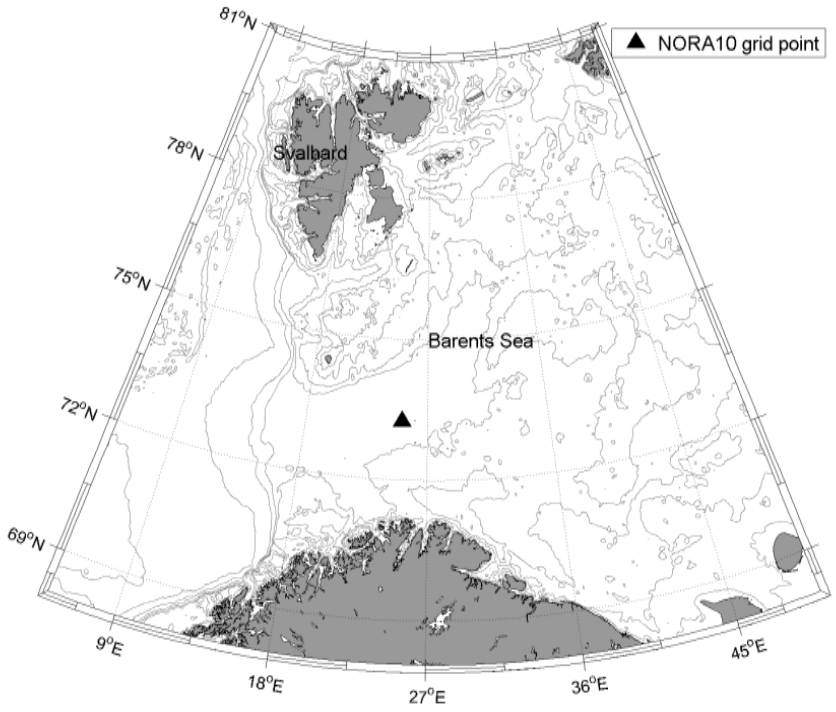

Figure 4. Map showing the location of the NORA10 hindcast grid point [25.10°E, 73.25°N] used in the case study.

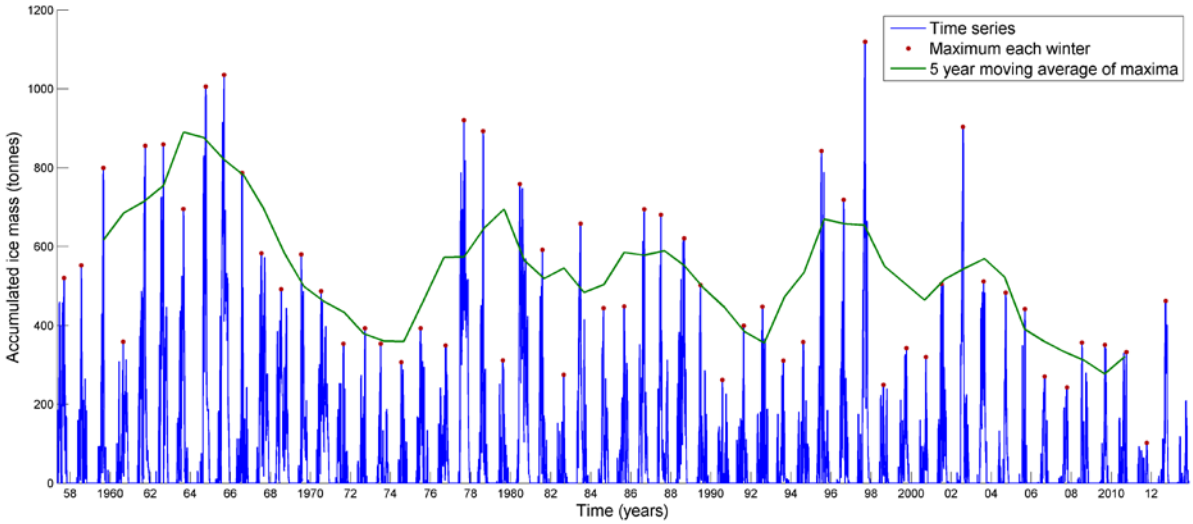

Figure 5. Time series of total accumulated ice load on the rig for the period 1957-2014. The maximal load each winter, as well as the moving average of maxima, are also indicated in the figure.

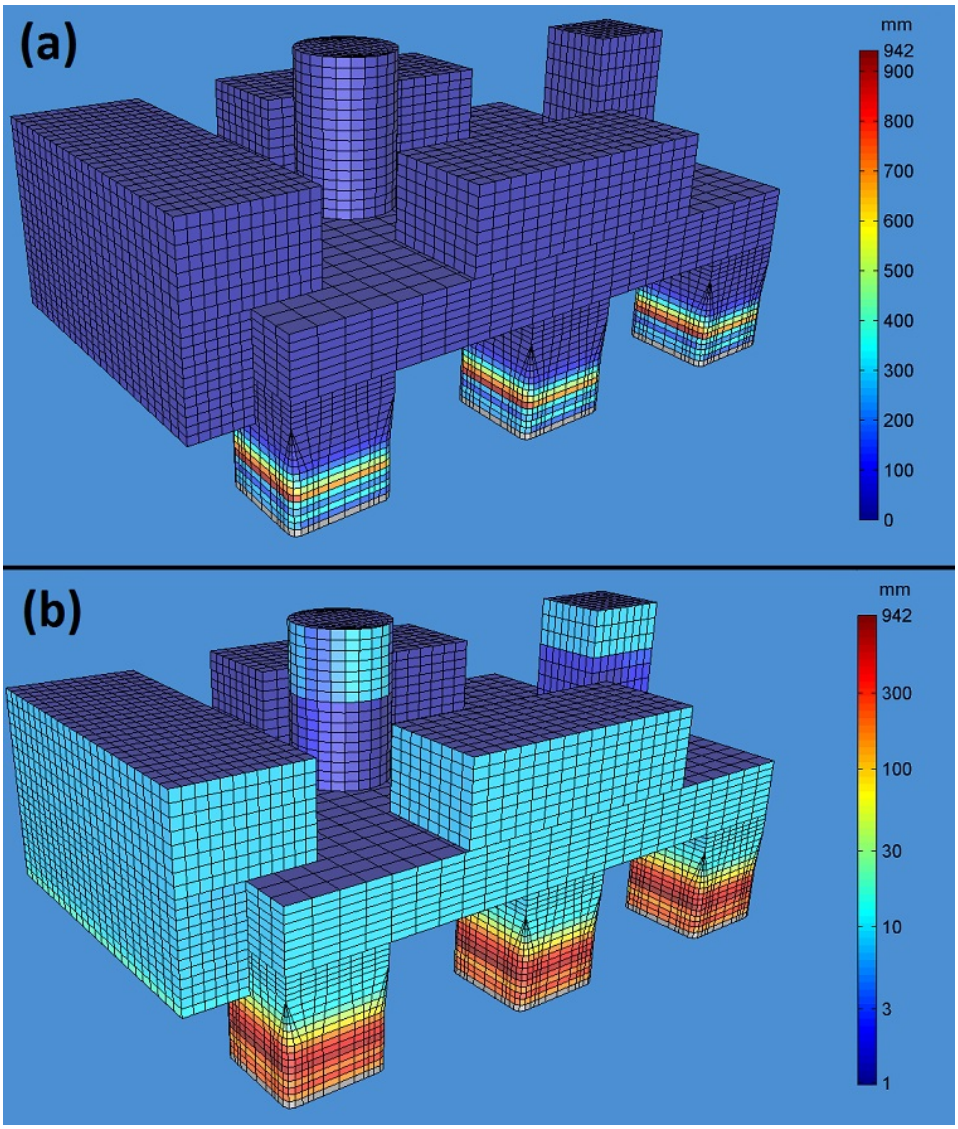

Figure 6. Distribution of ice thickness on the semi-submersible drilling rig during the event with the largest total ice mass (11th of March 1998), using a (a) linear and (b) logarithmic colour scale.

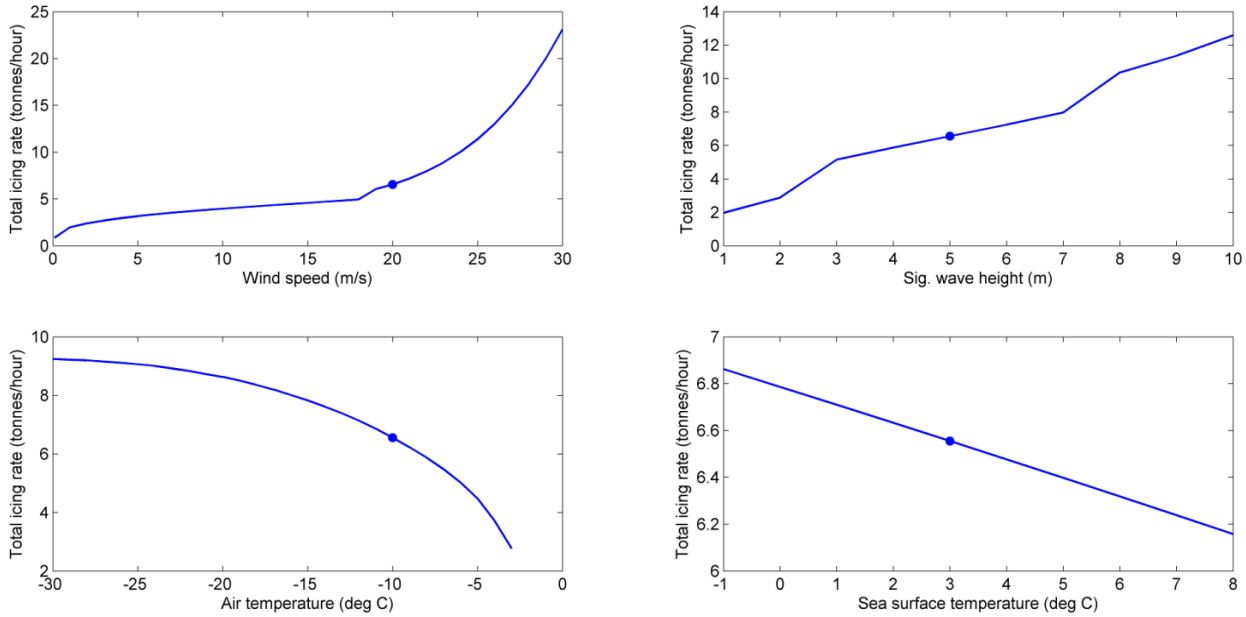

Figure 7. Dependency of icing rate to several key meteorological parameters, while all other parameters are kept constant. The round marker in each plot corresponds to the base case, as described in Table 1.

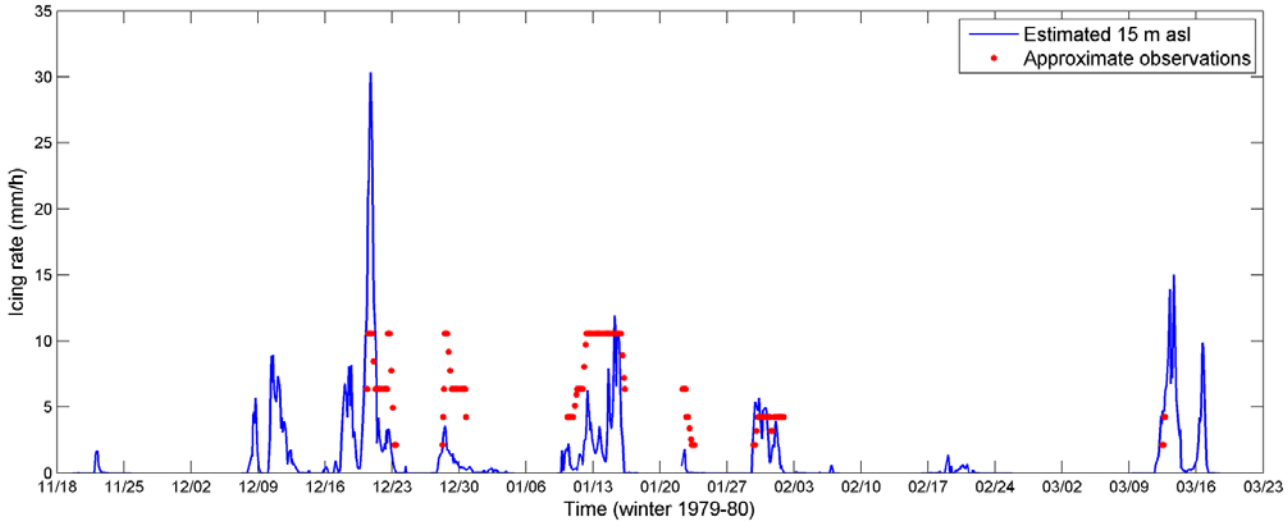

Figure 8. Time series of maximum icing rates at two height levels (5 m and 15 m above surface level) on the cylinder shown in Figure 7, using the meteorological and wave data registered at the Ocean Bounty rig during the 1979-1980 winter season. The approximate icing observations registered by the crew are also plotted.

REFERENCES

Blackmore, R. Z. & Lozowski, E. P., 1993. *An Heuristic Freezing Spray Model of Vessel Icing.* Singapore, Proceedings of the Third International Offshore and Polar Engineering Conference.

Churchill, S. W. & Bernstein, M., 1977. A Correlating Equation for Forced Convection From Gases and Liquids to a Circular Cylinder in Crossflow. *J. Heat Transfer,* pp. ASME 99: 300-306.

Defraeye, T., Blocken, B. & Carmeliet, J., 2010. Convective heat transfer coefficients for exterior building surfaces: Existing correlations and CFD modelling. *Energy Conversion and Management.*

Hansen, E. S., 2012. *Numerical modelling of marine icing on offshore structures and vessels,* s.l.: Master thesis, NTNU, Trondheim.

Horjen, I., 1990. *Numerical modelling of time-dependent marine icing, anti-icing and de-icing,* s.l.: Doctoral thesis, Norges Tekniske Høgskole, Trondheim.

Horjen, I. & Vefsnmo, S., 1985. *En kinematisk og termodynamisk analyse av sjøsprøyt,* s.l.: Norges Hydrodynamiske Laboratorier.

Jones, K. F. & Andreas, E. L., 2009. *Sea Spray Icing of Drilling and Production Platforms,* s.l.: Cold Regions Research and Engineering Laboratory, US Army Corps of Engineers.

Jones, K. F. & Andreas, E. L., 2012. *Sea spray concentrations and the icing of fixed offshore structures,* s.l.: Quarterly Journal of the Royal Meteorological Society.

Jørgensen, T. S., 1984. *Sjøsprøytmålinger på boreriggen "Treasure Scout" - Resultater fra forsøk april 1983 - februar 1984,* s.l.: Norges Hydrodynamiske Laboratorier.

Jørgensen, T. S., 1985. *Sea spray characteristics on a semi-submersible drilling rig,* s.l.: Norwegian Hydrotechnical Laboratory.

Kulyakhtin, A. e. a., 2013. *Measurements of Thermodynamic Properties of Ice Created by Frozen Sea Spray.* Anchorage, Alaska, USA, Proceedings of the Twenty-third (2013) International Offshore and Polar Engineering.

Kulyakhtin, A. & Tsarau, A., 2014. A time-dependent model of marine icing with application of computational fluid dynamics. *Cold Regions Science and Technology,* Volume 105-105, pp. 33-44.

Lozowski, E. P., Szilder, K. & Makkonen, L., 2000. *Computer simulation of marine ice accretion,* s.l.: Royal Society of London Philosophical Transactions Series A.

Løset, S. e. a. .., 2006. *Actions from Ice on Arctic Offshore and Coastal Structures,* St. Petersburg, Russia: Lan.

Nauman, J. W., 1984. *Superstructure icing observations on the semisubmersible Ocean Bounty in lower Cook Inlet, Alaska.* Trondheim, Second International Workshop on Atmospheric Icing of Structures, June 19-21, 1984.

Overland, J. E. e. a., 1986. Prediction of Vessel Icing. *Journal of Applied Meteorology ,* 25(12), pp. 1793-1806.

Reistad, M. et al., 2010. *A high-resolution hindcast of wind and waves for the North Sea, the Norwegian Sea, and the Barents Sea,* s.l.: J. Geophys. Res..

Ryerson, C. C. a. A. J. G., 2000. Crystalline structure and physical properties of ship superstructure spray ice. *Philosophical Transactions of the Royal Society of London. Series A: Mathematical, Physical and Engineering Sciences ,* 358(1776), pp. 2847-287.

Shipilova, O. et al., 2012. *Mechanism and Dynamics of Marine Ice Accretion on Vessel Archetypes.* Houston, Texas, USA, Arctic Technology Conference.